




Article

Measuring Dental Chamber Volume with DICOM Images from Cone-Beam Computed Tomography Can Be Improved with a Simple Algorithm

Lucía Hernández-Alvarez ¹, Iago Vila-García ², Zulima Fernández-Muñiz ², Ana Cernea ²,
Luis C. Hernández-González ¹, Teresa Cobo ^{3,4} and José A. Vega ^{1,5,*}

¹ Departamento de Morfología y Biología Celular, Universidad de Oviedo, 33006 Oviedo, Asturias, Spain; hernandezlucia@uniovi.es (L.H.-A.); lcarlos@uniovi.es (L.C.H.-G.)

² Departamento de Matemáticas, Universidad de Oviedo, 33007 Oviedo, Asturias, Spain; uo265800@uniovi.es (I.V.-G.); zulima@uniovi.es (Z.F.-M.); cerneadoina@uniovi.es (A.C.)

³ Departamento de Cirugía y Especialidades Medico-Quirúrgicas, Universidad de Oviedo, 33006 Oviedo, Asturias, Spain; teresacobo@uniovi.es

⁴ Instituto Asturiano de Odontología, 33006 Oviedo, Asturias, Spain

⁵ Facultad de Ciencias de la Salud, Universidad Autónoma de Chile, Providencia, Santiago 7500912, Chile

* Correspondence: javega@uniovi.es

Abstract: Knowledge of the precise anatomy and dimensions of the pulp chambers in different teeth allows the odontologist to perform correct diagnosis, as well as treatment planning and monitoring. Clinical practice has introduced cone-beam computed tomography (CB-CT) as a method to evaluate the morphology and dimensions of the pulp chamber. Nevertheless, micro-computed tomography (micro-CT) is regarded as the gold standard in approaching those topics. Here, we have designed an algorithm that takes as input DICOM images from in vivo CB-CT of permanent molars to determine the accuracy of CB-CT for evaluation of pulp chamber volume. The values were compared with those from in vivo CB-CT (rough and expert-manipulated) and ex vivo micro-CT. The relative errors obtained in the volume calculated by the algorithm vs. the volume measured by micro-CT did not exceed 5.7%; additionally, no significant differences were found between algorithm volumes and manipulated CB-CT volumes, while all volumes were different from those obtained with automatic CB-CT software. These data demonstrate that this CB-CT-based volume algorithm may be a reliable technique for evaluation of the pulp chamber volume in permanent molars and can be useful in the diagnosis of pulp diseases, as well as in the planning and monitoring of their treatments.

Keywords: cone-beam computed tomography; computed micro-tomography; dental pulp chamber volume; medical image; algorithm



Citation: Hernández-Alvarez, L.; Vila-García, I.; Fernández-Muñiz, Z.; Cernea, A.; Hernández-González, L.C.; Cobo, T.; Vega, J.A. Measuring Dental Chamber Volume with DICOM Images from Cone-Beam Computed Tomography Can Be Improved with a Simple Algorithm. *Appl. Sci.* **2024**, *14*, 5365. <https://doi.org/10.3390/app14135365>

Academic Editor: Hari Mohan Srivastava

Received: 14 May 2024

Revised: 12 June 2024

Accepted: 18 June 2024

Published: 21 June 2024



Copyright: © 2024 by the authors. Licensee MDPI, Basel, Switzerland. This article is an open access article distributed under the terms and conditions of the Creative Commons Attribution (CC BY) license (<https://creativecommons.org/licenses/by/4.0/>).

1. Introduction

Cone-beam computed tomography (CB-CT) has been introduced successfully in daily clinical practice. Small-field CB-CT makes it possible to obtain high-quality three-dimensional images of the teeth without the overlapping neighboring anatomical structures. This, associated with low radiation levels, has made CB-CT an imaging technique routinely used in diagnosis and planning of dental treatments [1–3]. One of the applications of CB-CT is the measurement of the pulp chamber from DICOM images. However, the values acquired show slight discrepancies with those obtained by micro-computed tomography (micro-CT). Micro-CT is currently regarded as the gold standard technique for assessing pulp chamber volume [4–8]. In addition, several factors limit the use of micro-CT in daily dental practice, including the high price of data analysis equipment and software, the time required for digital scanning and reconstruction, the limitations on the volume of samples it can analyze, and the high doses of radiation needed [1,5,9].

Therefore, the availability of reliable tools to measure the volume of the pulp chamber from CB-CT images, obtaining values as close as possible to those obtained by micro-CT, could be of great interest in daily clinical practice. Some studies are available that corroborate the accuracy and reproducibility of these comparative studies [10,11].

Therefore, the aim of this work was to design a simple algorithm capable of calculating the volume of the pulp chamber from DICOM images obtained with CB-CT. The results obtained show that its application makes it possible to obtain values almost identical to the real values measured by micro-CT. This is a validation of a method, not a quantitative study of a large series of samples.

This study was designed to validate the volume of the pulp chamber obtained using CB-CT in vivo (PromaxR 3D Max CBCT, Planmeca, Helsinki, Finland) by comparing it with the volumes obtained using micro-CT ex vivo. Dental treatments involving the dental chamber are becoming personalized, and the same tooth differs from one patient to another [12]. Thus, exact knowledge of the anatomy and volume of the dental chamber is essential to achieve successful treatments. This information is useful in various fields such as endodontics, forensic dentistry, and teaching.

2. Materials and Methods

Five permanent molars, corresponding to 5 subjects (3 females and 2 males), with ages ranging between 59 and 66 years, were analyzed. The teeth used in the study were programmed for exodontia due to different odontological treatments and were free of pulp chamber damage. This is the reason why the pulp chamber was intact and free of damage despite the age of the patients. It should be considered that teeth with caries suffer retraction of the pulp chamber, decreasing the volume of the pulp chamber. Likewise, restorations of decayed teeth produce artifacts in the images that prevent the volume from being correctly assessed. Additionally, molars were chosen due to their relatively large pulp chambers compared to other teeth. This characteristic made them ideal candidates for testing the algorithm's effectiveness.

Pieces were collected with written informed consent and obtained in accordance with Spanish legislation (RD 1301/2006; Law 14/2007; RD 1716/2011; Order ECC/1404/2013). Before exodontia, CB-CT images were obtained using tomographic equipment (ProMax3DMid ProFace, Planmeca, Helsinki, Finland), with a voltage of 120 kV and a tube current of 5 mA, except for the tooth identified as 5, for which the settings were 90 kV and 10 mA. For the analysis of DICOM (Digital Imaging and Communication in Medicine) images, the software used was Planmeca Romexis 6.2.1.25. Briefly, measurements were made as it follows: The axial and transverse axes were oriented according to the direction of the tooth. The tool "Measure a cube" was used to trace the area that covered the pulp chamber in the 3 views: axial, panoramic, and sagittal/orthoradial. A point inside the cube belonging to the pulp chamber was selected as the reference density for the "3D Growth Region" tool with the preset "Root Cavity", adjusting the threshold favorably (Figure 1a–d). To accurately determine the volume using CB-CT software (<https://anatomage.com/invivo/>, accessed on 1 March 2024), an expert observer's eye is essential for adjusting the threshold. The results obtained with the automatic threshold are less precise.

After exodontia, teeth were preserved in physiological saline solution at 4 °C until use for micro-CT study, which was carried out at the Centro Nacional de Investigacion sobre la Evolucion Humana (CENIEH; Burgos, Spain). The images were obtained with V|Tome|X s 240 from GE Sensing Inspection Technologies (Phoenix X-ray, Manufacturer: Baker Hughes, Celle, Germany), and for the analysis of the images, the software Dragonfly 2022.2 was used. The pulp canal was deleted from the rest of the tooth by adjusting the histogram. Once the pulp canals were isolated, a box was defined that corresponded to the region of the pulp chamber (Figure 1e–i). The software itself has a function that directly provides the volume value of the selected region (connected components; Figure 1i).

To calculate the pulp chamber volume, 300 DICOM images for each of the 5 samples, corresponding to different axial planes, were available. Nevertheless, only the images

corresponding to the pulp chamber were selected, resulting in a reduction of 14/300 for sample 1, 16/300 for sample 2, 9/300 for sample 3, 16/300 for sample 4, and 12/300 for sample 5. The selection was based on a meticulous visual analysis of each image by two experts, who established the initial and final planes containing parts of the pulp chamber. The image chosen as the initial one was the closest to the pulp canals among those that contained the pulp chamber, and the rest were selected in ascending order. On the other hand, the voxel size varied for each sample, with a side length of 0.25 mm for the first three samples, 0.2 mm for the fourth sample, and 0.15 mm for the fifth sample.

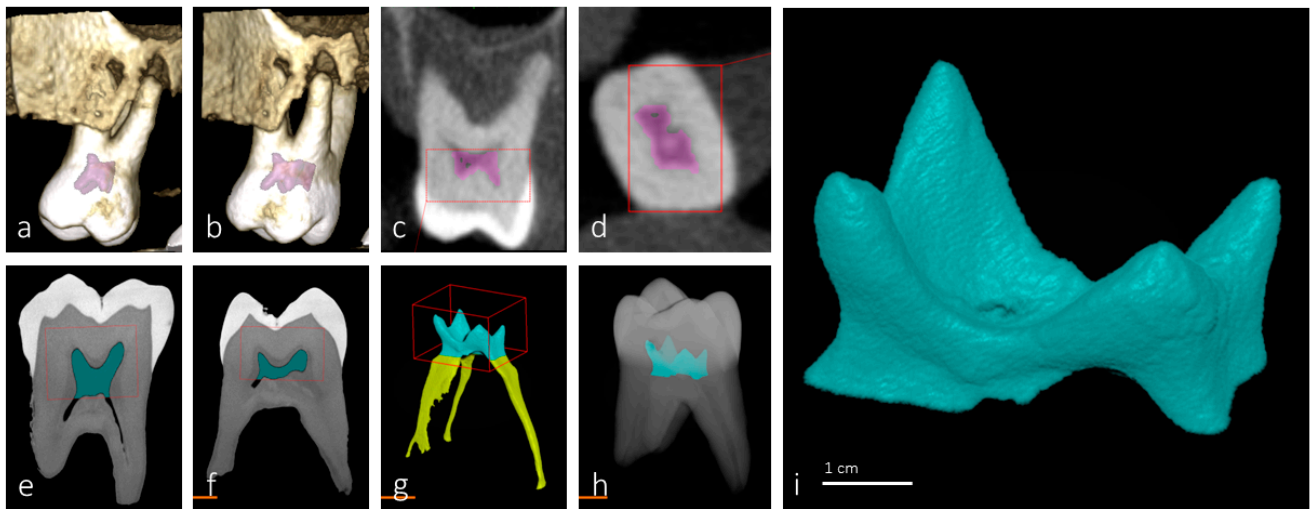


Figure 1. CB-CT and micro-CT images of the molar identified as sample 2 (corresponding to a female aged 62 years). CB-CT reconstruction (a,b) and sagittal (c) and axial (d) images. Micro-CT sagittal images (e,f) and pulp reconstructions (g,h). (i) corresponds to an isolated and enlarged detail of the pulp chamber shown in (h).

3. Design of the Algorithm

The effectiveness of image segmentation algorithms can vary depending on a range of factors, such as image complexity, image quality, the types of features being sought, noise present in the image, and the required accuracy for the specific task. In this case, a simple algorithm has been implemented to detect pixels belonging to the pulp chamber. Similar to any other image segmentation algorithm, it is based on the discontinuity or similarity between the gray levels of neighboring pixels, allowing it to locate changes in the gray levels of adjacent pixels. This algorithm can find isolated pixels, detect edges, and divide the image into zones that have similar gray values based on a certain threshold.

3.1. Preliminaries

The images used in this study are matrices in which each element corresponds to a position in the image (pixel). The value of each matrix element is determined by the color of the corresponding pixel (Figures 2 and 3). Since the images being used are in grayscale, each image is determined by a single matrix. Once the images are uploaded, an automatic check is performed to determine if the image has borders, and if so, they are not considered in the execution of the algorithm. This way, unnecessary calculations are avoided without preprocessing the images in the dataset.

Images 1–12 in Figures 2 and 3 correspond to different axial planes of samples 2 and 5, respectively. The portions corresponding to the pulp chamber are highlighted in blue, while the pulp chamber pixels detected by the algorithm are marked in red.

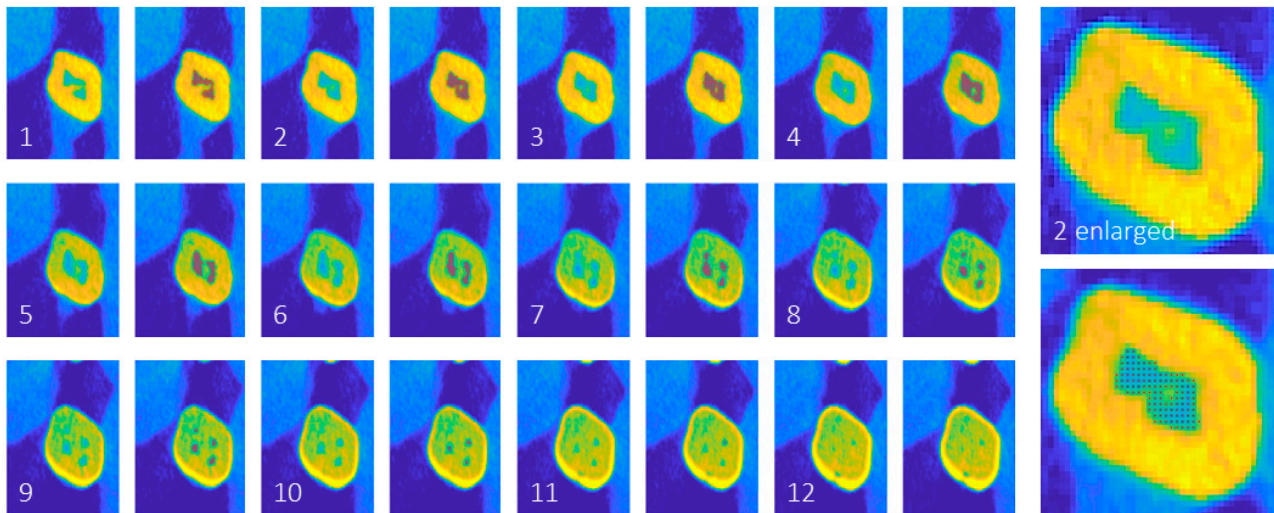


Figure 2. CB-CT images corresponding to the molar identified as sample 2. Axial images and area occupied by the pulp chamber (highlighted with red dots). In this sample, the algorithm values match those of micro-CT.

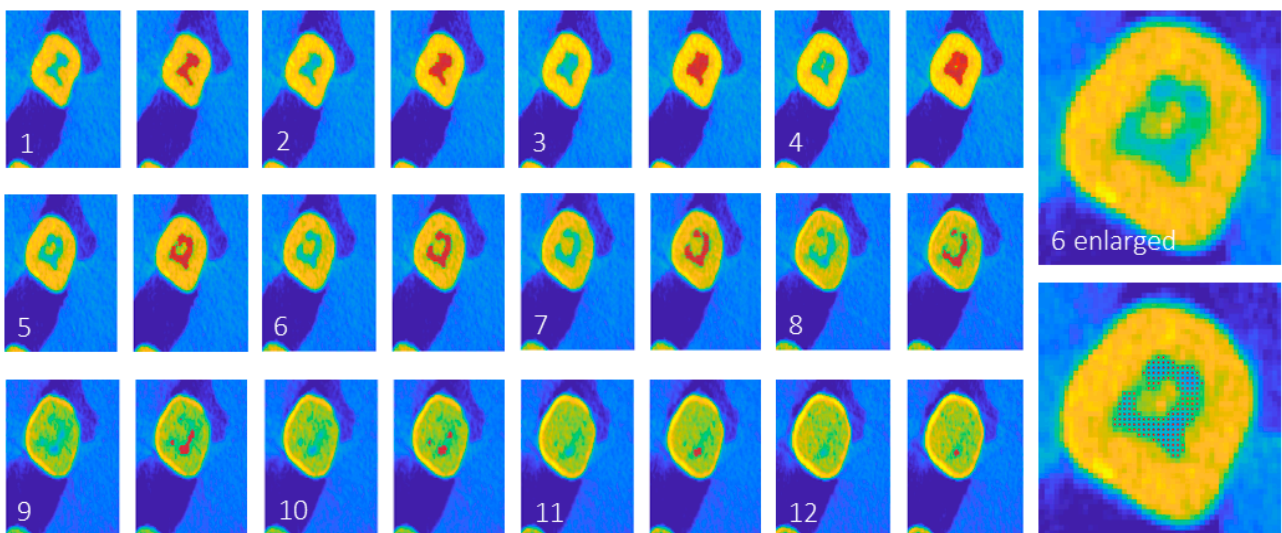


Figure 3. CB-CT images corresponding to the molar identified as sample 5. Axial images and area occupied by the pulp chamber (highlighted with red dots). In this sample, the algorithm values were very different from those of micro-CT.

The application d is defined as follows:

$$d : \mathbf{Z}^2 \rightarrow \mathbf{R}$$

$$x, y \rightarrow d(x, y) = |x_1 - y_1| + |x_2 - y_2| \tag{1}$$

where $x = (x_1, x_2), y = (y_1, y) \in \mathbf{Z}^2$, and (\mathbf{Z}^2, d) is therefore a metric space.

Given $\alpha \in \mathbf{N}$, on a set $A \in M_{2 \times N}(\mathbf{Z})$, the equivalence relation \sim_α is defined as follows:

$$x, z \in A \Rightarrow x \sim_\alpha z \Leftrightarrow \exists \{y_k\}_{k=1, \dots, N} \in A / \begin{cases} d(x, y_1) \leq \alpha \\ d(y_k, y_{k-1}) \leq \alpha, \quad k = 1, \dots, N - 1 \\ d(y_N, z) \leq \alpha \end{cases} \tag{2}$$

Given two elements $C_1, C_2 \in M_{2 \times N}(\mathbf{Z})$, the distance d_c between them is defined as follows:

$$d_c : M_{2 \times N}(\mathbf{Z}) \times M_{2 \times N}(\mathbf{Z}) \rightarrow \mathbf{R}$$

$$C_1, C_2 \rightarrow d_c(C_1, C_2) = \min(|x_1 - y_1| + |x_2 - y_2|) \tag{3}$$

where $(x_1, x_2) \in C_1$ and $(y_1, y_2) \in C_2$.

3.2. Algorithm Description

The main flowchart of the following algorithm is described in Figure 4. It consists of three phases, which are explained below:

1. Input elements

- Pixel matrix set: Each matrix corresponds to the image associated with a cross-section of the pulp chamber, in ascending order of height. It is understood that the first image corresponds to the first plane of the pulp chamber that does not include the molar canals.
- Pixel dimension: For each set of images, the unit of distance is the measurement of the pixel side. In turn, the inter-planar distance corresponds to the height of the pixel. For the sets considered, we work with cubic pixels (voxel).
- First surface point: To allow the detection of the pixels of the pulp chamber surface in the first matrix, it is necessary to consider a pixel belonging to it. If this pixel is not provided by the user, a pixel is selected automatically in the manner indicated below.
- Control parameter k (threshold): In the images considered, there is a color difference between pixels that belong to the bony surface of the tooth and those that do not. The control parameter k makes it possible to establish a prior separation between the elements of the pixel matrix that potentially belong to the pulp chamber and those that do not.

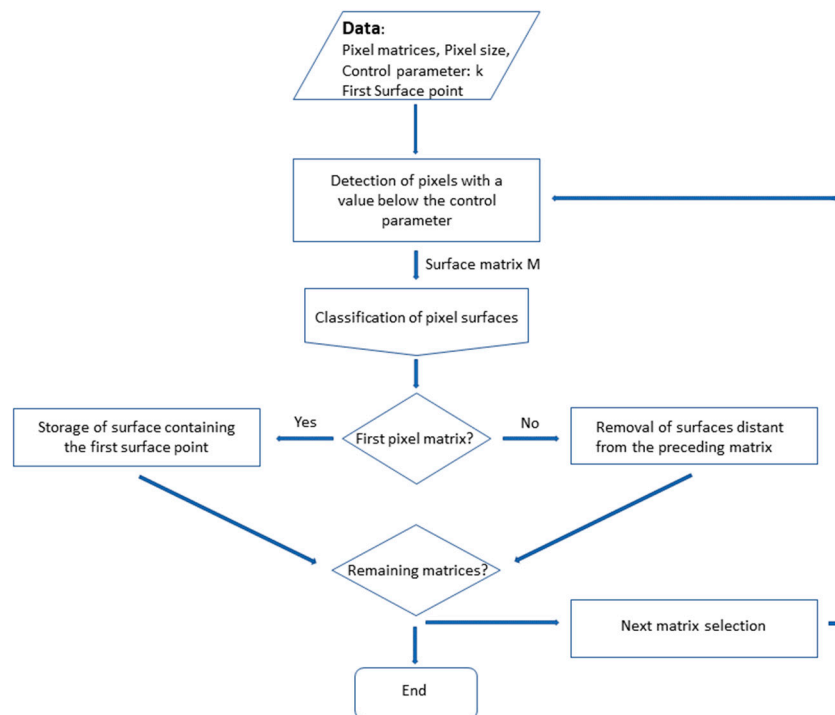


Figure 4. Main flowchart of the pulp chamber surface point detection algorithm.

2. Determination of the surface matrix

Starting from the pixel matrix I of each plane, a new matrix M (surface matrix) is constructed such that:

$$M_{ij} = \begin{cases} 1 & \text{if } I_{ij} \geq k \\ 0 & \text{if } I_{ij} < k \end{cases} \quad (4)$$

3. Calculation of pixel surfaces

Given a non-zero element a of matrix M of coordinates (a_1, a_2) , we define the equivalence class with representative a as $\{M_{ij} \in M / (i, j) \sim_2 (a_1, a_2) \wedge M_{ij} \neq 0\}$. Each of the equivalence classes is called a surface.

In the first step of the algorithm, a pixel of the pulp chamber is required. The first image, which is being worked with in the first step, is selected by an expert and is the closest to the molar canals. To identify the pixel belonging to the pulp chamber automatically, a pixel from the center of the image is selected first. If the pixel value is greater than the threshold value, it is considered to belong to the pulp chamber, and the algorithm is started. If the selected pixel is below the threshold value, the next closest pixel to the center of the image that has not yet been considered is taken, and the process is repeated.

Since the first image is the one closest to the molar canals, we are under the assumption that all pixels in the pulp chamber, in that plane, belong to the same equivalence class.

To separate each equivalence class, we begin by selecting a non-zero element in M (pixel) with coordinates P , from which we define a set S . This element is then set to zero in M . Next, we check if there are elements in M with coordinates P' that satisfy $d(P, P') \leq 2$ and are non-zero. If such elements exist, they are added to S , and the process is repeated for these new elements.

Once no more elements are added to S , the surface is considered complete, and a new non-zero element is taken in M . The algorithm ends when there are no more non-zero elements in M to add to an equivalence class.

At the end of the process, we have a separation of M into its different surfaces. The flowchart for this phase is shown in Figure 5.

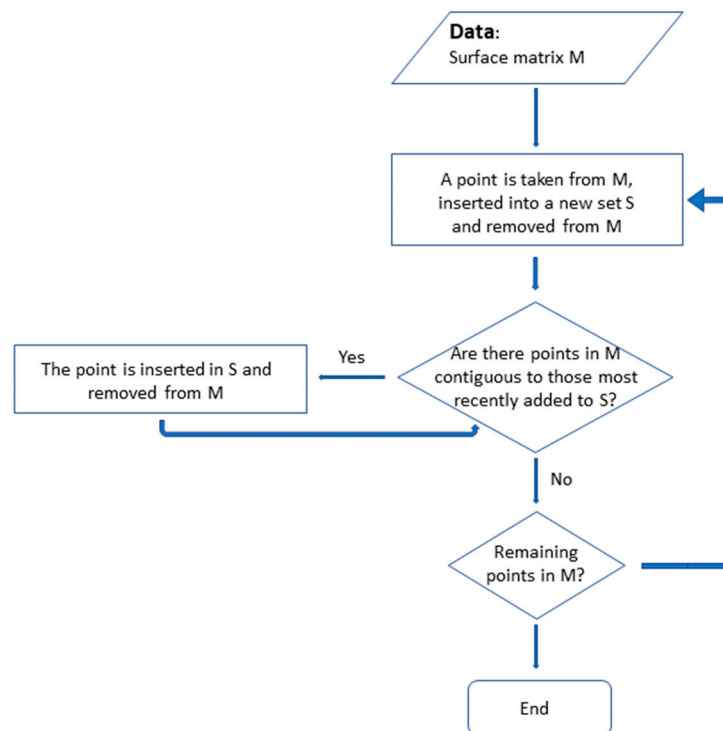


Figure 5. Main flowchart for calculation of pixel surfaces.

4. Identification of the pulp chamber

If it is the first image, only the surface containing the first surface point given as an input parameter is retained. If it is a subsequent image, surfaces far from those obtained in the previous iteration are eliminated. If S_j^i denotes the j -th surface in the i image, then:

$$S_j^i \in \text{pulp chamber} \Leftrightarrow \exists S_k^{i-1} / d_c(S_j^i, S_k^{i-1}) \leq 2 \tag{5}$$

At the end of each iteration, if new pixels associated with the pulp chamber have been obtained and if there are still images of the input set to be evaluated, we proceed to work with the next matrix. Otherwise, the volume calculation is performed.

3.3. Volume Calculation

The surface area of each pixel is the square of its side. Therefore, the value of the pulp chamber image area corresponding to each plane is the total number of pixels assigned to the pulp chamber multiplied by the individual surface area of the pixels.

For the calculation of the pulp chamber volume, two approaches are considered. In one case, the areas of the lower planes are taken and multiplied by the value of the distance between images (planes). In the other, the areas of the upper planes are multiplied by the distance between images.

Thus, considering a total of N images, in each case $N - 1$ volume values are obtained, one for each interplanar distance, the corresponding approximation being the sum of the calculated volumes. In this way, the two approximations of the volume are the extremes of an interval whose central value is the value of the volume considered, and the radius is the uncertainty in the measurement.

To attempt to estimate the algorithm's complexity, a study of its runtime was conducted under average conditions. For this purpose, the set of images associated with one of the samples was taken as representative and resized, while maintaining their aspect ratio, to sizes two, three, four, and five times the original size. To study the average runtime, one hundred measurements were taken for each group of images corresponding to a size. Through least-squares adjustment, cubic growth was identified (Figure 6).

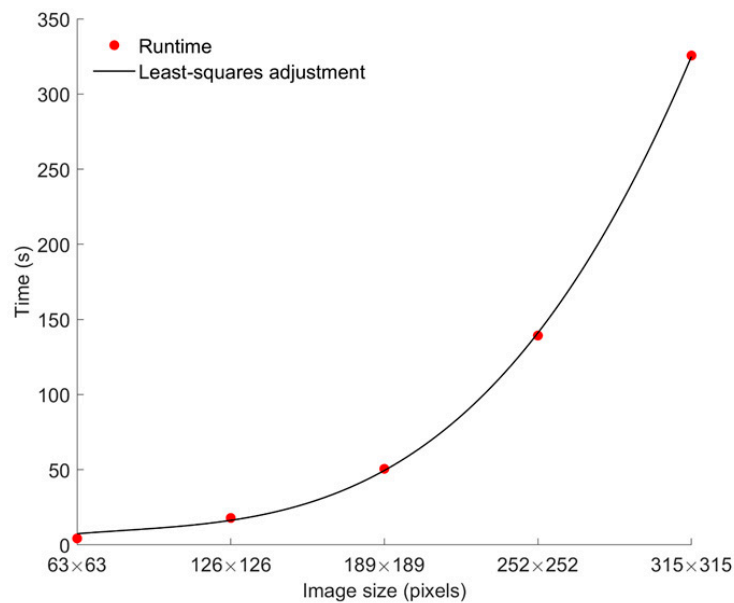


Figure 6. Average execution time as a function of the length of the image side.

Considering that the images processed in this case have a size smaller than 100×100 pixels, the average execution times obtained are just a few seconds. Thus, the functionality of the algorithm is proven, as it does not require waiting times to verify whether the result is

satisfactory. On the other hand, the observed behavior with the increase in the number of pixels makes it possible to understand the scalability of the algorithm to images with higher resolutions.

The average times were measured on a LAPTOP—AA7B78L5 Intel (R) Core (TM) i7-7500U CPU @ 2.70 GHz 2.90 GHz, with 8 GB RAM.

4. Results

The results with each method used in the study were obtained independently and by different analyzers and were supervised by two experts in the fields of dentistry and/or maxillofacial radiology, with extensive clinical experience to ensure the effectiveness of the procedure. The volumes of the pulp chamber according to the different methods used in the study are in Table 1. The data obtained with micro-CT were established as ideal and “true volumes” because of the high resolution of the images that were acquired due to the high dose of radiation used; those results were the most reliable.

Table 1. Comparative volumes obtained with the different methods used. 1: first; 2: second; M: molar. U: upper maxillary; L: lower maxillary. Software automatic threshold: 300.

	Micro-CT (mm ³)	CB-CT Viewer (mm ³) Set Threshold	CB-CT Viewer (mm ³) Automatic Threshold	CB-CT Algorithm
Sample 1 2MU	11.13	11	7	11.76 ± 0.6
Sample 2 1MU	11.79	13	8	12.4 ± 0.78
Sample 3 2ML	24.36	25	21	23.36 ± 1.26
Sample 4 1MU	14.1	9	4	14.36 ± 0.38
Sample 5 2MU	21.4	14	5	4.67 ± 0.22

The values obtained for samples 1, 2, and 4 were quite similar (Figure 2), while those for samples 3 and 5 were almost double (Figure 3). The range of the values was completely suitable and normal and was independent of the maxilla and place. From the CB-CT images manipulated by the specialist (set CB-CT threshold), the values were similar to those obtained by micro-CT except for samples 4 and 5, whose values were considerably lower. However, the volumes obtained with the automatic CB-CT threshold are always lower than those obtained with the established CB-CT threshold and with micro-CT, especially samples 4 and 5. Likewise, the volumes obtained with the algorithm are very similar to those obtained with micro-CT, with the exception of sample 5, whose value is very close to that obtained with the automatic CB-CT threshold, except for sample 3. The volumes generated by the mathematical formula resulted reliable in 4 of the 5 samples analyzed, with an error of 3.65% on average, and matched those obtained with micro-CT. Only in sample number 5 did the results calculated by the algorithm clearly differ from those obtained with micro-CT.

From the point of view of the algorithm, it can only be said that the method of detection of the pulp chamber is performed automatically using as data the distance between planes, the initial plane, and the control parameter k. For the algorithm to work, it is also necessary to know the location of a pixel belonging to the pulp chamber of the first image, which can be given by the user; otherwise, the central value of the image is taken. Based on these data, the pulp chamber is automatically detected in the planes where it exists, along with the corresponding volume. Therefore, from the perspective of the algorithm, there are no differences between sample 5 and the others (Figure 3); accordingly, it is not possible to justify the discrepancy between the volume provided by micro-CT and the calculated volume.

Several authors have calculated the pulp chamber volume for various purposes using different methods: one study measured the volume of the pulp cavity from cone-beam computed tomography (CB-CT) images by comparing them with the micro-CT reference standard, utilizing results from various radiological units and comparing 3D reconstructions using statistical methods [13]; some studies aimed to understand internal anatomy relationships prior to performing endodontic therapy using artificial intelligence techniques, training a U-Net network for automatic pulp segmentation [14,15]; one study calculated the pulp chamber volume for estimating human age using statistical methods [16,17]. The results obtained by the segmentation algorithm developed in this work, from the axial CT images, are comparable to those obtained in other works and easily reproducible, the only condition being that the first plane containing parts of the pulp cavity must be identified by an expert.

5. Discussion

The anatomy of teeth has been extensively studied and is globally well known. However, some aspects warrant re-analysis considering recent advancements in dental technology. One such aspect is the pulp chamber, as precisely understanding its anatomy and dimensions (particularly its volume) is crucial for accurate diagnosis, treatment planning, and monitoring [18].

This study was designed to validate the use of CB-CT for evaluating human pulp chamber volume using molars as a model. We compared *in vivo* CB-CT images—both raw and after manipulation by two trained experts and an algorithm—with *ex vivo* micro-CT images. Molars were chosen due to their large pulp chamber size [19]. The anatomy and dimensions of the pulp chamber are of interest in several dental fields, including endodontics [20,21], age estimation [22,23], dental pulp tissue engineering [24], and preclinical teaching and training of endodontic postgraduates [25,26].

An algorithm was developed to automatically calculate pulp chamber volume based on DICOM CB-CT images commonly used in dental clinics. The results demonstrate that the volumes obtained from *in vivo* CB-CT images differ from those obtained from *ex vivo* micro-CT images of the same teeth. However, the volumes were very similar when using the viewer-set CB-CT threshold and almost identical when processed with the algorithm, with relative errors not exceeding 5.7%. Therefore, the results suggest that *in vivo* CB-CT achieves high precision and reproducibility for evaluating pulp chamber volume when using the viewer-set threshold. The discrepancies between *in vivo* CB-CT and *ex vivo* micro-CT measurements may be partly due to the imprecision of CB-CT volumetric measurements caused by superimposed structures [2]. It should be noted that the measurements were obtained using only the Promax 3D Max CB-CT unit, and results could vary with other brands. Additionally, the Romexis Planmeca software offers a tool for pulp volume measurement, and the data obtained were included in the study.

The automatic volumes generated by the viewer with an automatic threshold differed significantly from those obtained by trained experts adjusting the threshold. Data obtained by threshold adjustment were much closer to the micro-CT data, indicating that the Romexis Planmeca viewer's automatic tool is not initially reliable for calculating dental pulp volume.

For samples 1 to 4, a voltage of 120 kV and a current of 5 mA were used, while for sample 5, 90 kV and 10 mA were used due to different scanner specifications. The voxel size also varied from 0.25 mm in the first three samples to 0.2 mm in the fourth sample and 0.15 mm in the fifth sample. These variations could explain significant differences between the volume results obtained by micro-CT and other methods [27,28].

The volumes obtained by adjusting the CB-CT image threshold closely matched those of the micro-CT, showing that dental pulp volume measurements are operator dependent. Despite keeping all parameters unchanged, notable discrepancies were found between the algorithm and micro-CT results in sample 5, possibly due to differing kV and mA settings and multiple pulp calcifications observed in the micro-CT images.

When calculating pulp chamber volume for sample 5 with the proposed algorithm and a voxel size of 0.2 mm, a volume of $11.06 \pm 0.52 \text{ mm}^3$ was obtained. However, using a voxel size of 0.25 mm resulted in a volume of $21.61 \pm 1.01 \text{ mm}^3$, highlighting the substantial influence of voxel size on measurements. While sample 5 showed discrepancies, similar calcifications in sample 3 did not affect alignment between micro-CT and algorithm results, indicating an unclear cause for these differences.

To our knowledge, this is the first study applying an algorithm with in vivo CB-CT to calculate dental pulp chamber volume and comparing it with ex vivo micro-CT results. However, the results should be interpreted cautiously due to the small sample size and differences between maxillary and mandibular molars [19]. Further studies are needed to explore other CB-CT brands and dental groups. Ongoing studies in our laboratory aim to validate CB-CT for volume measurements in different teeth using various CB-CT devices.

6. Conclusions

The study successfully demonstrates the efficacy of a simple algorithm for accurately measuring dental pulp chamber volume using DICOM images from cone-beam computed tomography (CB-CT). The algorithm's results closely matched those obtained using the gold standard, micro-CT, with relative errors not exceeding 5.7%. This algorithm offers a reliable, less invasive, and more accessible alternative for clinical dental practices, especially given the limitations of micro-CT, such as higher costs, longer processing times, and higher radiation doses.

The findings validate the idea that this algorithm can serve as a dependable tool for diagnosing and planning dental treatments involving the pulp chamber. It effectively bridges the gap between the convenience of CB-CT and the precision of micro-CT, thereby enhancing clinical decision making and patient outcomes. Further research with larger sample sizes and diverse dental conditions could solidify these findings and expand the algorithm's applicability across various clinical scenarios.

Author Contributions: Conceptualization, J.A.V. and Z.F.-M.; methodology, L.H.-A., I.V.-G., Z.F.-M. and J.A.V.; software, I.V.-G. and Z.F.-M.; validation, J.A.V. and Z.F.-M.; formal analysis, I.V.-G. and Z.F.-M.; investigation, L.H.-A., I.V.-G., Z.F.-M., L.C.H.-G., A.C., T.C. and J.A.V.; resources, L.H.-A.; data curation, J.A.V.; writing—original draft preparation, L.H.-A., I.V.-G., Z.F.-M. and J.A.V.; writing—review and editing, L.H.-A., I.V.-G., Z.F.-M., L.C.H.-G., A.C., T.C. and J.A.V.; visualization, L.H.-A., I.V.-G., Z.F.-M. and J.A.V.; supervision, J.A.V. and Z.F.-M.; project administration, Z.F.-M. and J.A.V.; funding acquisition, T.C. and J.A.V. All authors have read and agreed to the published version of the manuscript.

Funding: This research received no external funding.

Institutional Review Board Statement: Not applicable.

Informed Consent Statement: Informed consent was obtained from all subjects involved in the study.

Data Availability Statement: The data are not publicly available due to privacy.

Conflicts of Interest: The authors declare no conflict of interest.

References

1. Domark, J.D.; Hatton, J.F.; Benison, R.P.; Hildebolt, C.F. An ex vivo comparison of digital radiography and cone-beam and micro computed tomography in the detection of the number of canals in the mesiobuccal roots of maxillary molars. *J. Endod.* **2013**, *39*, 901–905. [[CrossRef](#)] [[PubMed](#)]
2. Fokas, G.; Vaughn, V.M.; Scarfe, W.C.; Bornstein, M.M. Accuracy of linear measurements on CBCT images related to presurgical implant treatment planning: A systematic review. *Clin. Oral. Impl. Res.* **2018**, *29*, 393–415. [[CrossRef](#)] [[PubMed](#)]
3. Asif, A.; Jeevanandan, G.; Govindaraju, L.; Vignesh, R.G.; Subramanian, E.M. Comparative Evaluation of Extrusion of Apical Debris in Primary Anterior Teeth using Two Different Rotary Systems and Hand Files: An In Vitro Study. *Contemp. Clin. Dent.* **2019**, *10*, 512–516. [[CrossRef](#)]
4. Nielsen, R.B.; Alyassin, A.M.; Peters, D.D.; Carnes, D.L.; Lancaster, J. Microcomputed tomography: An advanced system for detailed endodontic research. *J. Endod.* **1995**, *21*, 561–568. [[CrossRef](#)]
5. Rhodes, J.S.; Ford, T.R.; Lynch, J.A.; Liepins, P.J.; Curtis, R.V. Micro-computed tomography: A new tool for experimental endodontology. *Int. Endod. J.* **1999**, *32*, 165–170. [[CrossRef](#)]

6. Park, J.W.; Lee, J.K.; Ha, B.H.; Choi, J.H.; Perinpanayagam, H. Three-dimensional analysis of maxillary first molar mesiobuccal root canal configuration and curvature using microcomputed tomography. *Oral. Surg. Oral. Med. Oral. Pathol. Oral. Radiol. Endod.* **2009**, *108*, 437–442. [[CrossRef](#)]
7. Barsness, S.A.; Bowles, W.R.; Fok, A.; McClanahan, S.B.; Harris, S.P. An anatomical investigation of the mandibular second molar using micro-computed tomography. *Surg. Radiol. Anat.* **2015**, *37*, 267–272. [[CrossRef](#)]
8. De-Deus, G.; Belladonna, F.G.; Cavalcante, D.M.; Simoes-Carvalho, M.; Silva, E.J.N.L.; Carvalhal, J.C.A.; Zamolyi, R.Q.; Lopes, R.T.; Versiani, M.A.; Dummer, P.M.H.; et al. Contrast-enhanced micro-CT to assess dental pulp tissue debridement in root canals of extracted teeth: A series of cascading experiments towards method validation. *Int. Endod. J.* **2021**, *54*, 279–293. [[CrossRef](#)]
9. Michetti, J.; Maret, D.; Mallet, J.P.; Diemer, F. Validation of cone beam computed tomography as a tool to explore root canal anatomy. *J. Endod.* **2010**, *36*, 1187–1190. [[CrossRef](#)]
10. Maddalone, M.; Cittrio, C.; Pellegatta, A.; Gagliani, M.; Karanxha, L.; Del Fabbro, M. Cone-beam computed tomography accuracy in pulp chamber size evaluation: An ex vivo study. *Aust. Endod. J.* **2020**, *46*, 88–93. [[CrossRef](#)]
11. Barbosa, M.G.; Franco, A.; de Oliveira, R.D.B.; Mamani, M.P.; Junqueira, J.L.C.; Soares, M.Q.S. Pulp volume quantification methods in cone-beam computed tomography for age estimation: A critical review and meta-analysis. *J. Forensic Sci.* **2023**, *68*, 743–756. [[CrossRef](#)] [[PubMed](#)]
12. Schwendicke, F.; Samek, W.; Krois, J. Artificial Intelligence in Dentistry: Chances and Challenges. *J. Dent. Res.* **2020**, *99*, 769–774. [[CrossRef](#)] [[PubMed](#)]
13. Esteves Carneiro, A.L.; Spin-Neto, R.; Rabelo Mina Zambrana, N.R.; Rabelo Mina Zambrana, J.; Richarte de Andrade Salgado, D.M.; Costa, C. Quantitative and qualitative comparisons of pulp cavity volumes produced by cone beam computed tomography and micro-computed tomography through semiautomatic segmentation: An ex vivo investigation. *Oral. Surg. Oral. Med. Oral. Pathol. Oral Radiol.* **2023**, *135*, 433–443. [[CrossRef](#)] [[PubMed](#)]
14. Duan, W.; Chen, Y.; Zhang, Q.; Lin, X.; Yang, X. Refined tooth and pulp segmentation using U-Net in CBCT image. *Dentomaxillofac. Radiol.* **2021**, *50*, 20200251. [[CrossRef](#)] [[PubMed](#)]
15. Lin, X.; Fu, Y.; Ren, G.; Yang, X.; Duan, W.; Chen, Y.; Zhang, Q. Micro-Computed Tomography-Guided Artificial Intelligence for Pulp Cavity and Tooth Segmentation on Cone-beam Computed Tomography. *J. Endod.* **2021**, *47*, 1933–1941. [[CrossRef](#)]
16. Ge, Z.P.; Ma, R.H.; Li, G.; Zhang, J.Z.; Ma, X.C. Age estimation based on pulp chamber volume of first molars from cone-beam computed tomography images. *Forensic Sci. Int.* **2015**, *253*, 133.e1–133.e7. [[CrossRef](#)]
17. Elgazzar, F.M.; Elboraey, M.O.; El-Sarnagawy, G.N. The accuracy of age estimation from pulp chamber/crown volume ratio of canines obtained by cone beam computed tomography images: An Egyptian study. *Egypt. J. Forensic Sci.* **2020**, *10*, 40. [[CrossRef](#)]
18. Liu, Y.; Olszewski, R.; Alexandroni, E.S.; Enciso, R.; Xu, T.; Mah, J.K. The validity of in vivo tooth volume determinations from cone-beam computed tomography. *Angle Orthod.* **2010**, *80*, 160–166. [[CrossRef](#)] [[PubMed](#)]
19. Dieguez-Perez, M.; Ticona-Flores, J.M. Three-Dimensional Analysis of the Pulp Chamber and Coronal Tooth of Primary Molars: An In Vitro Study. *Int. J. Environ. Res. Public Health* **2022**, *19*, 9279. [[CrossRef](#)]
20. Van der Meer, W.J.; Vissink, A.; Ng, Y.L.; Gulabivala, K. 3D Computer aided treatment planning in endodontics. *J. Dent.* **2016**, *45*, 67–72. [[CrossRef](#)]
21. Ahmed, H.M.A.; Ibrahim, N.; Mohamad, N.S.; Nambiar, P.; Muhammad, R.F.; Yusoff, M.; Dummer, P.M.H. Application of a new system for classifying root and canal anatomy in studies involving micro-computed tomography and cone beam computed tomography: Explanation and elaboration. *Int. Endod. J.* **2021**, *54*, 1056–1082. [[CrossRef](#)] [[PubMed](#)]
22. Molina, A.; Bravo, M.; Fonseca, G.M.; Marquez-Grant, N.; Martin de Las Heras, S. Dental age estimation based on pulp chamber/crown volume ratio measured on CBCT images in a Spanish population. *Int. J. Legal Med.* **2021**, *135*, 359–364. [[CrossRef](#)] [[PubMed](#)]
23. Zheng, Q.; Ge, Z.; Du, H.; Li, G. Age estimation based on 3D pulp chamber segmentation of first molars from cone-beam-computed tomography by integrated deep learning and level set. *Int. J. Legal Med.* **2021**, *135*, 365–373. [[CrossRef](#)]
24. Hadjichristou, C.; About, I.; Koidis, P.; Bakopoulou, A. Advanced in Vitro Experimental Models for Tissue Engineering-based Reconstruction of a 3D Dentin/pulp Complex: A Literature Review. *Stem Cell Rev. Rep.* **2021**, *17*, 785–802. [[CrossRef](#)] [[PubMed](#)]
25. Hohne, C.; Schmitter, M. 3D Printed Teeth for the Preclinical Education of Dental Students. *J. Dent. Educ.* **2019**, *83*, 1100–1106. [[CrossRef](#)] [[PubMed](#)]
26. Hohne, C.; Schwarzbauer, R.; Schmitter, M. Introduction of a new teaching concept for crown preparation with 3D printed teeth. *Eur. J. Dent. Educ.* **2020**, *24*, 526–534. [[CrossRef](#)] [[PubMed](#)]
27. Maret, D.; Telmon, N.; Peters, O.A.; Lepage, B.; Treil, J.; Inglese, J.M.; Peyre, A.; Kahn, J.L.; Sixou, M. Effect of voxel size on the accuracy of 3D reconstructions with cone beam CT. *Dentomaxillofac. Radiol.* **2012**, *41*, 649–655. [[CrossRef](#)]
28. Maret, D.; Peters, O.A.; Galibourg, A.; Dumoncel, J.; Esclassan, R.; Kahn, J.L.; Sixou, M.; Telmon, N. Comparison of the accuracy of 3-dimensional cone-beam computed tomography and micro-computed tomography reconstructions by using different voxel sizes. *J. Endod.* **2014**, *40*, 1321–1326. [[CrossRef](#)]

Disclaimer/Publisher’s Note: The statements, opinions and data contained in all publications are solely those of the individual author(s) and contributor(s) and not of MDPI and/or the editor(s). MDPI and/or the editor(s) disclaim responsibility for any injury to people or property resulting from any ideas, methods, instructions or products referred to in the content.